To the Graduate Council:

I am submitting herewith a dissertation written by Ryan W. Kapler entitled "Elastic Scattering of Deuterons on ^{132}Sn in Inverse Kinematics." I have examined the final electronic copy of this dissertation for form and content and recommend that it be accepted in partial fulfillment of the requirements for the degree of Master of Science, with a major in Physics.

Kate Jones, Major Professor

We have read this dissertation
and recommend its acceptance:

Mike Guidry

Carrol Bingham

Accepted for the Council:

Carolyn R. Hodges, Vice Provost
and Dean of the Graduate School

(Original signatures are on file with official student records.)

The Elastic Scattering of Deuterons on ^{132}Sn

A Dissertation

Presented for the

Master of Science

Degree

The University of Tennessee, Knoxville

Ryan W Kapler

May 2009

Copyright © 2008 by Ryan W Kapler.
All rights reserved.

Dedication

For family, friends, and colleagues that have helped me along the way, this is the sum of your efforts

Acknowledgments

I would like to first acknowledge the committee members for allowing me to present this thesis and also for withstanding the scheduling of the defense process. Truly I doubt there has been more reschedulings for one event in the history of man. Further, I would like to acknowledge, my advisor, Dr. Kate Jones. Her guidance and encouragement throughout this project were constant and unfaltering. Her method of always allowing to let me try and swim on my own when starting a new aspect of this research gave me the confidence to take on and complete this project. This project is the centerpiece of an unique and eye opening experience that has been my grad school career.

I would like to acknowledge the University of Tennessee's department of Physics and Astronomy for a top notch education and teaching experience.

I would like to acknowledge Jolie Cizewski and the Center of Excellence for Stewardship Science. Their support made this work possible.

Next I would like to list a few personal acknowledgments:

Jay Jay Billing- You know there is too much to be listed here. So when I say thanks for everything, it pretty much means everything.

Brain "Maddog" Moazen- Thanks for showing me the ropes at ORNL and always letting me know what's what, even when I didn't care.

Andy Chae- For always having an answer for any off the wall question I came up with and wearing those awesome solid color shirts.

Meredith- You have been my anchor, shelter, and partner in crime. I could not have done this without your support. There is no way I can replay you...well maybe during your 4th year at vet school.

Abstract

Half of the elements heavier then iron are produced in the rapid neutron capture (r-) process. The final abundances of the r-process are determined not only by masses and beta-decays of nuclei on the path, but also neutron capture reaction rates. The structure of neutron-rich nuclei close to the r-process needs to be further investigated and this can be accomplished using the (d,p) reaction. However, conventional experimental methods do not allow for short-lived exotic neutron-rich nuclei to be probed via a (d,p) reaction, as they cannot be made into a target. Using inverse kinematics and radioactive ion beams (RIB) produced by the Holifield Radioactive Ion Beam Facility (HRIBF) at Oak Ridge national laboratory, (d,p) reactions can be used to investigate exotic neutron-rich nuclei. Three such experiments were performed at ORNL: ^{132}Sn(d,p)^{133}Sn, ^{130}Sn(d,p)^{131}Sn, and ^{134}Te(d,p)^{135}Te. These experiments were possible due to the availability of the RIBs and to the implementation of the Oak Ridge Rutgers University Barrel Array (ORRUBA). ORRUBA allows for symmetric large solid angle coverage about 90 degrees. Since ORRUBA is a new detector system, a new gain matching routine needed to be developed for it, as older methods extrapolated from other detector systems were less then optimal. Since the RIB is focused onto a CD_2 target there are three possible elastic scattering reactions. In this thesis the ^{132}Sn(d,d)^{132}Sn reaction in particular was studied. The analysis showed that the scattering was not purely Rutherford scattering. After comparing several optical models it was clear that an optical potential based on the scattering data from isotopes located close to ^{132}Sn best fit the elastic data. The analysis of the elastic scattering data was used to verify the optical potential used and to provide a normalization for the (d,p) reaction.

Contents

List of Figures

Chapter 1

Introduction

1.1 Motivation

Currently the nuclear structure of exotic neutron-rich nuclei is not well known. Most of the knowledge of exotic neutron-rich nuclei has come from the extrapolation of studies of nearby stable isotopes. While the shell model works well in describing stable nuclei, there is some debate over whether or not it can accurately describe exotic nuclei. The (d,p) reaction can be used to probe the nuclear structure of these neutron-rich nuclei. As more (d,p) experiments are performed on these nuclei, a better understanding of their underlying structure can be obtained.

1.2 The (d,p) transfer reaction

A (d,p) reaction is a one neutron transfer reaction. In the conventional set-up a target is made of a stable isotope. A deuteron beam is focused onto the target. The target nuclei then absorbs the neutron from the deuteron, leaving the proton, which is measured. Since the deuteron is so loosely bound, (d,p) reactions can be used to model neutron capture. While (d,p) reactions can be used to study a whole range of stable or near stable nuclei, more exotic nuclei were, until recently, out of reach. In the conventional method the nuclei must make up the target. However, focusing a radioactive beam of an unstable nucleus onto a deuteron target, i.e. performing the reaction in inverse kinematics, will solve this problem. With the use of this experimental setup it is possible to study (d,p) reactions with

nuclei far from stability. This will allow for more experimental testing of nuclear structure models in nuclei far from stability. It pushes the limitations from only being able to use stable nuclei to the types of radioactive beams that can be produced. Three mass 130 experiments were run at ORNL: ^{132}Sn(d,p)^{133}Sn, ^{130}Sn(d,p)^{131}Sn, and ^{134}Te(d,p)^{135}Te.

1.3 Elastic Scattering Reactions

In the reverse kinematics setup the target is not made of purely deuterons. It is mostly mixture of CD_2 and a little CH_2. Due to this make up of the target there are three possible elastic scattering reactions. For example in the ^{132}Sn experiment the following elastic scattering was observed, ^{1} H(^{132}Sn,^{132}Sn)^{1}H,^{2}H(^{132}Sn,^{132}Sn)^{2}H, and ^{12}C(^{132}Sn,^{132} Sn)^{12}C, for shorthand purposes these will be referred to as (p,p), (d,d), and (^{12}C,^{12}C) respectively. The statistical data from these scattering reactions will be used for normalization purposes and to select the best optical model for spectroscopic factor extraction. This thesis covers the work required to analyze the ^{132}Sn(d,d) elastic scattering data collected concurrently with ^{132}Sn(d,p) data. This includes calibration techniques and routines written that allowed the analysis of both channels with improved resolution over previous methods.

Chapter 2

Theory and Background

2.1 Shell Model

Throughout history, scientists have used models to describe complex systems. Nuclear physicists are no exception. In developing a model of a complex system such as a nucleus it is best to begin with a general, and in some cases oversimplified, model. When a simple model that can mathematically describe general properties of the system on the macroscopic scale is in place then extra terms can be added to improve the model on the microscopic level [Kra88a]. In developing the nuclear model nuclear physicists began with the atomic shell model as their oversimplified model."Atomic theory based on the shell model has provided remarkable clarification of the complicated details of atomic structure. Nuclear physicists therefore attempted to use a similar theory to attack the problem of nuclear structure..." [Kra88b]. In the atomic shell model electrons fill shells in order of increasing energy and also satisfying the Pauli exclusion principle. When this is done the trend that is seen in the atomic shell model is a core of filled shells with valence electrons left over in the outer unfilled shells. The model suggests that these valence electrons play a crucial role in the atomic properties of the atom. In the atomic shell model smooth and regular differences in the ionic radius and ionization energy are seen in elements as the outer most shell is filled, however sudden changes are seen when a shell is filled and the next shell is available. Due to the strong correlation with experimental data the atomic shell model is widely accepted. Therefore the atomic shell model made sense as a starting

point when nuclear physicists decided to derive the nuclear shell model. However, there were some objections to simply extrapolating the atomic shell model. The shells of atomic electrons are defined by an external Coulomb potential of the nucleus, in a nucleus this potential is created by the nucleons themselves. Also the orbits of the electrons are large when compared to the size of the electron. These spatial orbits allow the electron to move free of collisions with other electrons. In comparison, the orbits within a nuclear model would be much smaller when compared to a nucleon's diameter, therefore a nuclear shell model needs to account for the many collisions that a nucleon may undergo while moving within it's defined orbit. And lastly a nuclear shell model must support two shell hierarchies, a shell structure for protons and another for neutrons. Initially there was debate on whether the shell model could describe a system where the potential is generated by the particles themselves, like the nucleus. The potential for the nuclear shell model is dealt with by considering a single nucleon moving in a potential created by all the other nucleons. This consideration allows for the potential to be modeled as an external potential from the perspective of the nucleon, but as internal from the perspective of the nucleus. The existence of shells is because of the Pauli exclusion principle. Even though these shells will be small when compared to the size of nucleons, collisions between nucleons in the same shell are generally disregarded in the nuclear shell model. Let's consider a heavy nucleus, for which many of the shells will be filled according to the Pauli principle. If a collision occurs between two nucleons in a low-energy shell then classically some energy transfer would occur. However, since the shells are filled up until the outer valance shell there is no way quantum mechanically for one of the nucleons to gain energy unless it populates the valence level. It is unlikely that a collision in a low-lying level will transfer enough energy to either nucleon for this to happen. Therefore the nucleons are assumed to orbit as freely as the electrons in the atomic shell model [Kra88a]. Experimental data have supported the adoption of the simplified shell model as the nuclear model. In fact the data have revealed several traits that are now of interest to nuclear physicists. As N and Z increase small and smooth increases are seen in neutron or proton separation energy. However, when certain numbers of nucleons are reached there is a sudden rise in separation energy. This is analogous to the ionization energy changes seen in the atomic model that correspond to electron shell closures. It suggests that these "magic" numbers

(N or Z = 2, 8, 20, 28, 50, 82, and 126) correspond to closed shells of proton or neutrons. When a nucleus has a closed shell of protons or neutrons it is referred to as "magic". If both neutron and proton shells are closed, then the nucleus is said to be "doubly magic". While these magic numbers corresponded very well to data from nuclei close to the valley of stability, variances in nuclear structure of exotic neutron-rich nuclei have been seen. Tests of the shell model are therefore required for exotic nuclei. Neutron-induced nuclear reactions on unstable neutron-rich nuclei, especially those near closed neutron shells, are thought to be important in determining the reaction flow in the astrophysical r-process in supernovae [B$^+$08].

2.2 Nucleosynthesis

Nucleosynthesis is the process of creating new nuclei from existing lighter nuclei, protons, and neutrons in stars and explosive cosmic events such as novae and supernovae. Depending on the mass of the stars, H and He are used as fuel in nuclear fusion until A $\approx$ 60. Beyond this mass fusion reactions are not energetically favored [Kra88c]. However, heavier nuclei do exist, therefore production methods must occur for heavier nuclei. At this point to further increase the mass of nuclei, neutron capture is the primary production mechanism. Neutron capture followed by beta decays is the method for increasing atomic number in both the slow (s-) and rapid (r-) neutron capture processes. [Kra88c]. Iron is the most abundant element found near the mass 60 fusion barrier, of which ^{56}Fe is the most abundant stable isotope. At this point only neutron capture can achieve heavier isotopes. If there is sufficient neutron flux density then through (n,γ) reactions ^{59}Fe is attainable. ^{59}Fe is radioactive, with a half life of 45 days. If the neutron flux is low enough that the probability of neutron capture within 45 days is sufficiently small then it will beta decay to stable ^{59}Co; which then through neutron capture will become radioactive ^{60}Co. If the neutron flux is so high that neutron capture will occur before beta decay then (n,γ) reactions can occur until the half life is so short that neutron capture can not occur before decay. The first process in which neutron capture takes a long time, the slow neutron capture or s-process, is thought to occur inside stars, while the latter process involving quick neutron captures, the r-process, occurs in the more explosive environment such as supernovae [RR88]. The

s-process is limited by beta-decay half-lives. When the s-process reaches a nucleus that has a beta decay half-life much shorter than time required for neutron capture then it has reached the limit. This limit occurs around the stable isotopes of ^{208}Pb and ^{209}Bi. To reach the heavier stable isotopes and stable actinides beyond the limit of the s-process, the r-procress is the only option.

2.3 The r-process

Due to the necessity of an extreme high neutron flux for the r-process, the environment during the core collapse of a supernova and neutron star collisions are thought to be the possible sites for the r-process. This incredibly high neutron flux allows the r-process to reach extremely neutron-rich isotopes, far from the valley of stability. Since the r-process is responsible for the production of approximately half the elements heavier than Fe, it plays a key role in calculating abundances of elements. The r-process nucleosynthesis calculations depend primarily on masses and beta decay half lives. However it has been shown recently that neutron capture rates can play a key role in calculating final abundances of the r-process [B$^+$08], [S$^+$08]. Currently it's not possible to make reliable calculations as the vital nuclear physics input comes from a shell model that has been extrapolated from stable regions where measurements exist into this unstable exotic region, where it is not well tested. To achieve better calculations of r-process nucleosynthesis better masses, beta-decay half-lives, and neutron capture rates are required. To improve the nuclear structure model these exotic nuclei must be investigated. Previously experiments to investigate this region were limited. However, with radioactive beams and the use of inverse kinematics, the structure of exotic doubly-magic nuclei and nuclei related to them by adding or subtracting a single nucleon (single-particle and single-hole nuclei) can be studied. Improvements and adjustments to the nuclear shell model will help to improve r-process nucleosynthesis calculations.

2.4 Elastic Scattering

In general, scattering theory is the outlining framework use to understand the scattering of waves and/or particles. It is possible to divide scattering theory up into a great many subsets based on the types of particles or waves involved and also the area of physics or mathematics interested in the scattering. However, the primary and most fundamental division in scattering theory is to classify it as elastic or inelastic scattering. With elastic scattering the kinetic energy of the system of particles is conserved, as opposed to inelastic scattering in which the kinetic energy is not conserved. The (d,d) and (^{12}C,^{12}C) reactions analyzed here fall into the the elastic scattering subdivision. The nucleus has a charge distribution. When considering nuclear reactions all particles involved besides neutrons are positively charged [Sat90]. This feature means that the interactions between particles in nuclear reactions are governed by two forces, the repulsive Coulomb and the nuclear force, which is attractive for the energies relevant for this work. The nuclear, or strong, force governs the interaction between nucleons. It arises from the strong interaction that holds quarks and gluons together to form nucleons. Each nucleus has essentially a two-part potential. At large distances this potential is dominated by the repulsive Coulomb potential. At much smaller scales this potential is dominated by the attractive nuclear force. Therefore as charged particles are scattered off a nucleus the resultant scattering pattern is a mixture of nuclear and Coulomb effects.

2.4.1 Rutherford Scattering

As stated above, because of the charge distribution of the nucleus part of the scattering of particles is due to the Coulomb potential. Elastic Coulomb scattering, or Rutherford scattering, is often used as a tool to study nuclei. Particles will travel towards a nucleus along a trajectory which can be approximated initially by a straight line. The particle's path is parallel to the line that runs directly through the nucleus and is offset by a distance b, called the impact parameter. If there was no repulsive force the particle would simply pass by the nucleus at the distance b. However, there is a repulsive force and the particle is deflected. The Coulomb force between the particle with charge Z_1e and the nucleus with a charge Z_2e is $Z_1Z_2e^2/\mathrm{r}^2$, where r is the distance between the two particles [Sat90].

As is the case with the geometry for unbound orbits in a $1/r^2$ force, the particle follows a hyperbolic path [Kra88d]. In careful consideration of the nucleus it is evident that an azimuthal symmetry exists, therefore the scattering angle will not have a dependence on the azimuthal angle, ϕ. Using conservation of energy, angular momentum, and the properties of hyperbolae the Rutherford cross section can be derived [Sat90]. The differential cross section is expressed as:

$$\frac{d\sigma}{d\Omega} = \left(\frac{Z_1 Z_2 e^2}{4\pi\epsilon_o}\right)^2 \left(\frac{1}{4E_{c.m.}}\right)^2 \left(\frac{1}{\sin^4 \frac{\theta_{c.m.}}{2}}\right) \tag{2.1}$$

Where $E_{c.m}$ and $\theta_{c.m}$ represent the initial kinetic energy of the incoming particle and the scattering angle, respectively, in the center of mass frame, ϵ_o is the permittivity of free space constant and e is the magnitude of electric charge of the electron. Observing equation 2.1, it is evident that the angular distribution has a universal form and the scale of the cross section only depends on the charge of the particles, the charge on the nuclei, and the bombarding energy. Typically in textbook derivations of the Rutherford cross section the assumption of the target being much more massive then the particle is made, this is done to make the recoil of the target negligible. However by changing to the center of mass coordinate system, as equation 2.1 is shown, this assumption is not needed.

2.4.2 Nuclear Scattering

The elastic nuclear scattering pattern of particles bears a strong resemblance to scattering patterns in another area of physics, optics. With elastic nuclear scattering the pattern seen is characterized by a high intensity at small angles followed by a quick drop off. This pattern is repeated with decreasing intensities for each peak. This peak followed by a valley pattern mirrors a typical diffraction pattern. Since scattering is azimuthally symmetric the complete elastic nuclear scattering picture is an intense central region or peak surrounded by alternating concentric rings of peaks and valleys. Due to the similarity to diffraction the nucleus can be thought of as an opaque glass sphere [Kra88d]. The target nucleus is a good absorbing object for nucleons, therefore for charged particles, such as the deuteron, elastic scattering is not simple to analyze. There is interference between the nuclear and Coulomb scattering. To accurately describe the interference of the Rutherford scattering

and absorption due to nuclear effects an optical model is adopted [Kra88d].

2.4.3 The Optical Model

The optical model derives its name because the calculations involved resemble that of light incident on a opaque glass sphere [Kra88d]. It is a model used to account for elastic scattering in the presence of the absorptive effects of the nucleus. It treats the scattering, as resulting from a complex potential. In general the potential $U(r)$ has a form:

$$U(r) = V(r) + iW(r) \tag{2.2}$$

Since there is no angular dependence, the potential depends only on the radial coordinate, r. The $V(r)$ term is responsible for modeling the elastic scattering, while the $W(r)$ term is responsible for the absorption [Kra88d]. There are essentially two types of optical models used in modeling elastic scattering. Models that are based on data from many nuclei in the mass range of the experiment are considered "global", while optical models based on one or few nuclei are considered "local". Both global and local optical models were considered in the analysis of the ^{132}Sn(d,d) data.

Chapter 3

Experimental

3.1 Detector Setup

3.1.1 ORRUBA

The Oak Ridge Rutgers University Barrel Array (ORRUBA) is a large solid angle silicon detector array for measuring proton ejectiles from transfer reactions. It is composed of two rings of twelve position-sensitive silicon detector telescopes, as seen in figure 3.1. The physical design of ORRUBA allows for symmetric angular coverage of forward and backward laboratory angles around 90°, with respect to the target. At forward angles telescopes composed of two detectors are required to enable particle identification. The first is a thin transmission detector, also referred to as a delta energy (ΔE) detector. The transmission detectors have a thickness of 65 or 140 μm. The transmission detectors are mounted in front of thicker stopping detectors, or energy (E) detectors. The stopping detectors are 1000 μm thick. Using these detector telescopes with ORRUBA allows for the collection of energy, angle, and particle identification. ORRUBA can be used in conjunction with other detector systems and arrays to provide larger angular coverage. The Silicon Detector Array (SIDAR) [B^+00] and QQQ's are two of the arrays that are used with ORRUBA. SIDAR is a silicon strip detector system consisting of 6 or 8 wedge shaped silicon strip detectors. Each wedge is comprised of 16 radial divisions covering radii 5 cm to 13 cm from beam line. SIDAR can be mounted either upstream or downstream from a target such that its aperture is centered on the beam line. Another feature of SIDAR is its ability

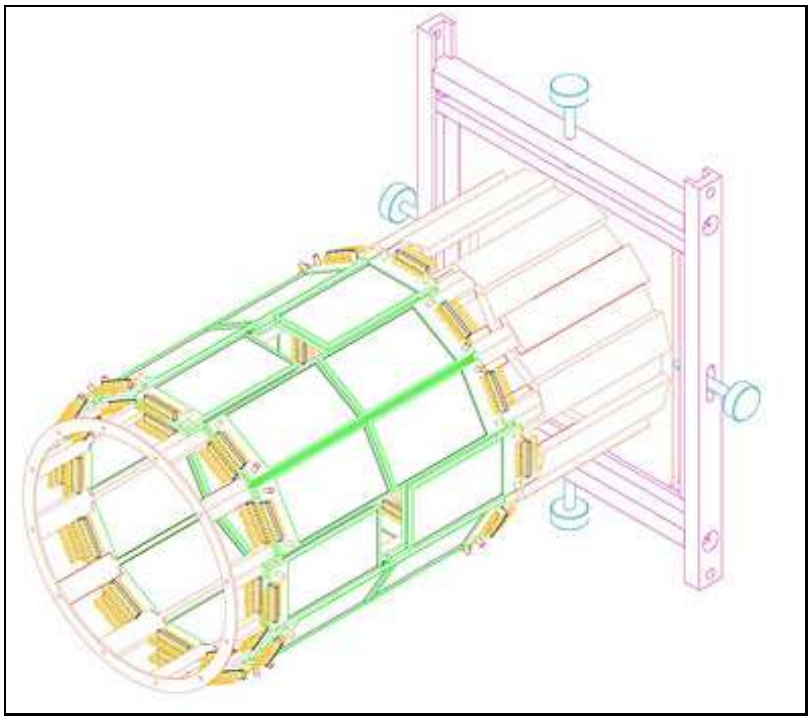

Figure 3.1: The Oak Ridge Rutgers University Barrel Array configured with 12 ORRUBA detector telescopes. Also depicted in pink is the mounting system for the array.

to be mounted flat or in a lampshade configuration. SIDAR is similar to ORRUBA as it also employs a telescope design, however, unlike ORRUBA it is not position sensitive. The angle of the detected particle is given by the strip it was detected in. It can however be mounted and used with one, two, or three layers of detectors, depending on the logistics of the experimental setup. QQQ is a detector system that can be used much like SIDAR, except it has a smaller aperture, thus allowing it to detect even smaller angle reactions products. Due to ORRUBA's compact design and detector coverage specifically around the target it does not interfere with these other detector systems. In simpler terms, since ORRUBA is a barrel array around the target, SIDAR and QQQ can be thought of as end caps for the barrel.

3.1.2 ORRUBA Detectors

The detectors used in ORRUBA are position-sensitive silicon detectors. Each ORRUBA detector is 7.5 cm long 4 cm wide. The surface of the detector is divided into 4 strips

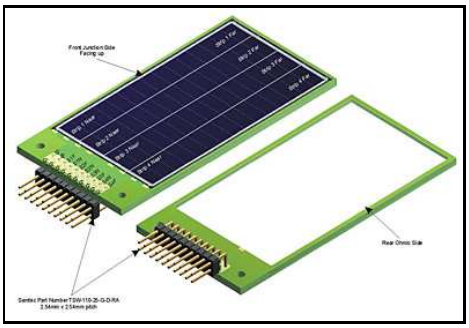

Figure 3.2: Surface view of typical ORRUBA detector.

with each strip having dimensions of 7.5 cm by 1 cm, as seen in figure 3.2. The position sensitivity of the detector comes from charge division due to a resistive layer. During an event each end of the strip records a signal. The sum of these signals for one strip gives the energy deposited by the particle. Since the strips are resistive, the position on the strip of the event can be determined from calculating the difference of the signals at each end divided by the energy. With the detectors in telescope configuration the total energy of the particle is a sum of the energy measured in the transmission detector and the stopping detector. The full ORRUBA can accommodate twelve detector telescopes in each hemisphere, at the time of the ^{132}Sn(d,p) experiment, however, only a fraction of these detectors were available. ORRUBA detector telescopes were placed where the emission angles were of particular interest. Four ORRUBA telescopes were placed in forward angle positions. Included with the ORRUBA telescopes was the PSD/PAD telescope. The PSD detector, shown in figure 3.3, is a position-sensitive detector that is 5 cm long and 5 cm wide. It is divided into 16 resistive strips and should offer better resolution than the ORRUBA detectors. The PAD is a 5 cm by 5 cm single layer detector that is not position sensitive. For backward angle measurements 6 ORRUBA stopping detectors were used. Angular coverage for the experiment was as follows; the four forward telescope detectors of ORRUBA and the PSD covered laboratory(center of mass) angles from $69^{/circ}$ to 107°(31° to 70°), the six backward ORRUBA detectors covered from 90° to 130°(18^o to 46°), and SIDAR was mounted in lampshade configuration and covered lab angles from 143° to 167°(4°to 12°).

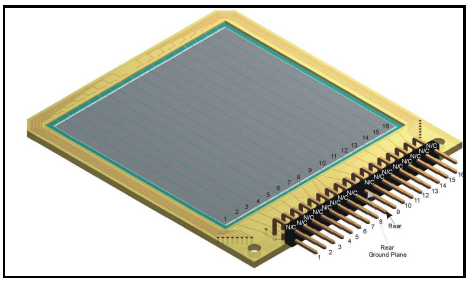

Figure 3.3: Surface view of the 5x5 PSD. It was used in conjunction with a non position sensitive stopping detector to create a higher resolution telescope for forward angle coverage.

3.2 Electronics Chain

During the (d,p) experiments a series of electronic units were used. The electronics needed to be located close to the detectors to preserve signal integrity. The electronics chain reliably identifies good events, converts them, transmits them, and stores them. This process begins with the signals from the detectors. The raw signals from the detectors are sent to a pre-amplifier. This pre-amplifier boosts the raw signals and routes them to a shaping amplifier. For real events the signal is proportional to the charge collected at one end of the detector. The shaping amplifier creates a fast digital discriminator signal, which is not proportional to energy. The shaping amplifier then sends the analog feed to the Analog to Digital Converter (ADC), and the newly created digital signal is routed to a series of trigger modules. The trigger modules are wired to the ADC so that when the digital feed corresponding to a real event is present the trigger modules will trigger the ADC to accept the analog feed from the shaping amplifier. The ADC will then convert the analog data to digital. This digital data is ready to be recorded to disk. The last component in the electronics chain, is the Virtual Machine Environment (VME). The VME is a way for the acquisition computer to send feedback to the electronics chain. The VME interacts with the acquisition computer where data are collected.

3.3 Radioactive Ion Beam Production

As already iterated previously the key to studying these (d,p) reactions on unstable nuclei is the use of a Radioactive Ion Beam (RIB). Though this thesis will not delve in-depth

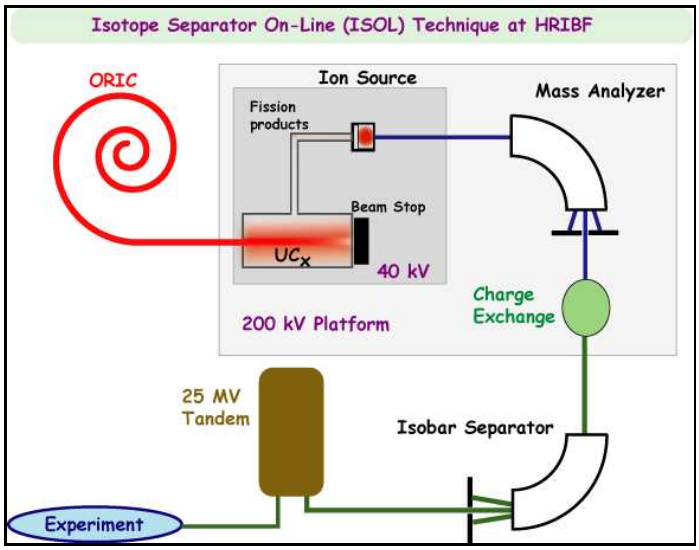

Figure 3.4: Simple cartoon of the RIB production method at HRIBF.

into RIBs, they are important enough to the work presented here that a brief description of RIB production is warranted. RIBs are produced at the Holifield Radioactive Ion Beam Facility (HRIBF), via the Isotope Separator On-Line Production (ISOL) method. ISOL begins with the production of radioactive isotopes. These radioactive isotopes are created by protons accelerated by the Oak Ridge Isochronous Cyclotron (ORIC) and focused onto an uranium carbide target. This causes the ^{238}U to fission into a range of isotopes. The isotopes flow out of the target and are accelerated across a potential of 40 kV. The isotopes are directed into a mass analyzing magnet. The desired isotopes for the RIB can be selected by tuning the magnetic field of the mass analyzer. The selected isotopes are then passed through a charge exchange-cell. In the charge exchange cell electrons are acquired by the radioactive ions. A higher-resolution mass analyzer, the Isobar Separator, further purifies the beam before directing it to the tandem accelerator. The 25 MV tandem accelerator is the post acceleration method for the RIB. Negative ions from the charge exchange cell are accelerated to the high voltage positive terminal at the top of the 100 ft van der Graaf accelerator to produce the RIB. An electron stripping foil at the top of the tower removes the recently acquired electrons. The newly positive RIB is then accelerated away from the positive terminal. The RIB is then directed to the experimental set-up. Figure 3.4 is a "cartoon" of the HRIBF production process [HRI].

3.4 Gain Matching

3.4.1 Importance of Gain Matching

Each channel of electronics in the (d,p) experiments was set up similarly, however it is not possible to get exactly equal gains from electronic chains. Therefore it is necessary in all experiments to gain match. When using position sensitive strip detectors the signals from the two ends must be summed and compared to extract position and energy of particles. Without properly calibrating the data, accurate analysis is impossible. Optimum gain matching allows for optimum resolution, which in turn yields more effective analysis of the collected data.

3.4.2 Gain Matching Procedure

When mono-energetic alpha-particles illuminate a strip on a detector, the sum of the two ends will equal that energy. When the signal from one end is plotted against the other end the expected plot is a straight line with a gradient of negative one and intercepts each axis at the energy of the alpha particle. The mono-energetic source of alpha particles used for gain matching during the (d,p) experiments was ^{244}Cm. The energy of the alpha particles is 5.8 MeV. Data were collected from each detector while being illuminated by the ^{244}Cm. The data were then scanned and sorted into histograms, that can be read by DAMM (Display and Manipulation Module). While there are many good features of DAMM, the fitting of 2D histograms was not. The goal of the gain fitting project was to create a systematic method for gain matching the ORRUBA detectors. The mass $\sim$ 130 (d,p) experiments were the first ones for which ORRUBA was used extensively, as a result there was not an optimized method for gain matching the array. Previous methods only looked at the extremes of the distribution and were imprecise in the selection of the points used to fit the data. This method is outdated for the ORRUBA detectors. The flaws in the older methods caused several problems in the gains. Since the selection is dependent on the user, the gains obtained by the older method are unique to the user. Also if the line of the data plot is not straight then the gains will be biased towards the extremes and detrimental to the fit. This new gain matching method was developed to overcome these shortcomings of the older method. By specifically working with ORRUBA detectors the

new method is better equipped to deal with the problems and qualities. This insured that the new method was first optimized to deal with ORRUBA and could be easily applied to other detector systems.

3.4.3 The Method

The first goal of the calibration method is to ensure that the data sample used to calibrate the detectors is not limited to a few points selected 'by eye'. To optimize the calibration method it was decided that the base size of data to use in calibration should at first contain all the data. Another required property of the calibration method was a manual filtering option to cut out any artifacts that began appearing in the data. And the last and most vital property of the new calibration method is to apply a robust fit to the data. To extract the data from the histogram file the SPKHIS, a c++ program was used [Var]. It takes a user supplied histogram identification number and writes the data for the histogram to a data file. For a 2D histogram SPKHIS outputs a three column ASCII file. SPKHIS writes this information for every possible point in the plot, for example a 512 channel by 512 channel histogram would generate a 262144 line data file. The vast majority of the points would correspond to empty space and be of little interest. On average with the ^{132}Sn calibrations these large data files only contain a few hundred points of interest. To gain match the output files of SPKHIS, I wrote a new gain matching program, RKUSF. RKUSF is a Fortran 90 code that works in three steps on the ungain-matched data files. The first step is to unpack the data file. RKUSF first reads the header line of the user specified data file. SPKHIS records the total number of lines of each data file as the first line in the file. RKUSF reads this line to allocate an array large enough to store the entire data file. Next RKUSF will scan through the data and filter some points out based on user-defined parameters. There are two filtering options within RKUSF. The first and most basic is a noise threshold. The noise filtering threshold allows the user to set a parameter that will eliminate data points with values below threshold. Since this threshold is user defined and applied to the entirety of the raw data the user has control over how much data is filtered. The second data filtering option was added because an artifact started to present itself. In some of the detectors a large artifact was observed near the origin, as seen in

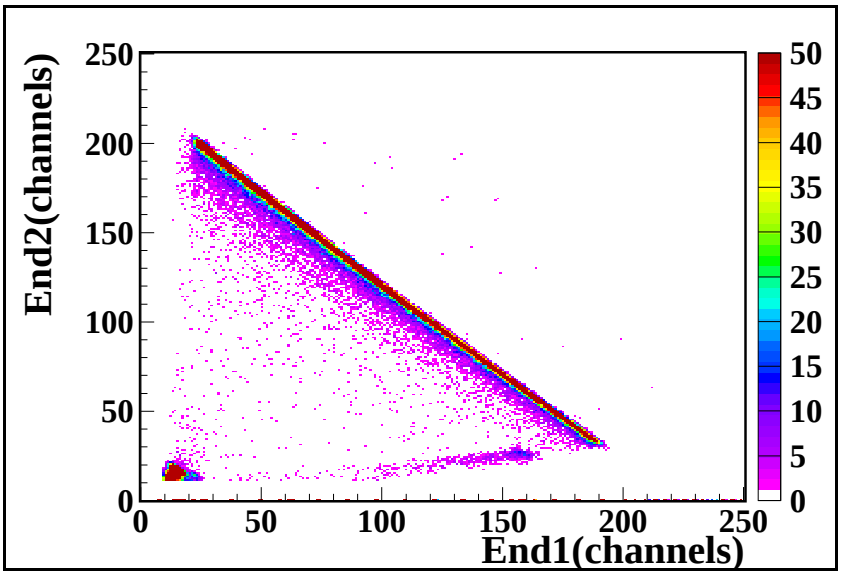

Figure 3.5: A plot of ungain-matched data, collected in the forward angle E detector. Notice how the intensity of the artifact near the origin is equal to that of the end vs end line. Establishing a threshold high enough to eliminate the artifact would also filter all the other data plotted as well.

figure 3.5. Often the artifact would reach high intensities. It is thought that these artifacts are a result of electronic noise. As seen in figure 3.5, the intensity of these artifacts is comparable to the End vs End line. The noise threshold is picked so that it will eliminate noise. Looking at figure 3.5, a threshold of fifteen would filter out everything except for the End vs End line and artifact near the origin. Since these objects are have comparable intensities, simply applying a higher noise filtering threshold would filter out the artifact and also the data of interest. This artifact is handled with a second feature of RKUSF, a cutting line. The cutting line takes points selected by the user and formulates an equation for a straight line containing those points. A second option of instructs RKUSF to filter out data above or below the line. The combination of the noise threshold and the cutting line allows the user to easily select the relevant data for the calibration. After the raw data has be narrowed to useful and interesting points, RKUSF is ready to fit the data. RKUSF applies a linear least squares fit to the selected data. The fitting routine is the standard least squares fit from Numerical Recipes [PTVF92].

3.4.4 Least Squares Fitting

Least squares fitting a straight line to a collection of data depends on by a few simple ideas. First is that there are two sets of N data points, defined by a dependent variable, y, and an independent variable, x. A model, with parameters is used to describe the data. For a straight line the model involves two parameters, the gradient m and the intercept b. The fit is determined by the minimization of a chi-squared function. For fitting a straight line the equation for the model and the chi-squared function are, equations 3.1 and 3.2, respectively.

$$y(x) = y(x; b, m) = mx + b \tag{3.1}$$

$$\chi^2(b, m) = \sum_{i=1}^{N} (y_i - b - mx_i)^2 \tag{3.2}$$

3.4.5 Development of Gain Equations

After RKUSF fits the data, the equation for the best fit straight line for that data is known. Due to the way that RKUSF, and more so SPKHIS, handle the data, end 1 is considered the x value, and end 2 is the y value. For simplicity in the following section the terms x and y will be used for these values. Mathematically, the fit line describes a plotting trend from set of x and y data points. With gain matching, two factors are developed to shift the data, one for the x values and one for the y values. Applying the factors to the data and re-fitting will yield a best fit line that has the correct gradient and intercept. There are two steps to developing the gain factors. First the gradient must be fixed, then the intercept can be adjusted. The equation from RKUSF for the best fit line is of the general from of equation 3.3. The gains need to make the data fit a line of the form of equation 3.4, with m' and b' being the ideal values. To fix the gradient equation 3.3 is multiplied by the desired slope over the uncorrected slope. Now that the gradient is fixed a second factor is used to fix the intercept, it has the form of b' times m over b times m'. After these steps have been carried out equation 3.3 will now have the form of equation 3.5. The factors in front of x and y are the gain coefficients. G_x and G_y are the general form of the required gains to change the best fit line from equation 3.3 to 3.4. Using these constants, the parameters of the initial fit line and the general form of the gain factors, RKUSF was

able to calculate the gains for both ends of every strip for each detector used in the set up.

$$y = mx + b \tag{3.3}$$

$$y' = m'x' + b' \tag{3.4}$$

$$\underbrace{\left(\frac{b'}{b}\right)}_{\mathrm{G}_y} y = m' \underbrace{\left(\frac{b'm}{bm'}\right)}_{\mathrm{G}_x} x + b' \tag{3.5}$$

$$y' = G_y y \tag{3.6}$$

$$x' = G_x x \tag{3.7}$$

3.5 Elastic Scattering

3.5.1 Gates and Angular Distributions

The statistical analysis of the elastic scattering data began with the careful selection of the data using user-created gates. The scan code was altered so that the angle and energy values for the histogram were written out to a data file. XMGrace, a 2D plotting tool for the X window system, was used to carefully look at this data file to insure that the design of the gates for the scattering reactions were precise. The gates for each reaction had four sides. The top and bottom boundaries were decided by the alpha line and the point at which the data began to converge around the 90° mark. The left and right boundaries where defined by parabolic equations defined by hand picked sets of points from the XMGrace analysis. Initially it was thought that the (^{12}C,^{12}C) reaction gate needed to be divided into two gates since the alpha line cuts the data in half. However, after looking at the constant value for a one degree bin it was determined that the alpha contamination would not significantly affect the (^{12}C,^{12}C) reaction. With the gates defined the scan code was altered for angular distribution binning. Gated data were sorted into a series of histograms. Each histogram represents one of the angular bins, and therefore the number of counts in the histogram represents the number of particles scattered into the detector at that angle. The plotting of these values against the angles they correspond to generates an angular distribution for the elastic scattering. Initially a calculation for the ^{132}Sn(d,d)^{132}Sn reaction using equation

2.1 was plotted against the angular distribution. It was clear that points generated from the bins in the middle of the angular distributions seemed to agree with the general trend of the calculated line, but points at the ends of the data did not. After looking at the data in XMGrace with the gate lines it was clear that these points near the ends of the angular range were suffering from "clipping". The gate box drawn around the reaction, as described above, can be viewed roughly as a parallelogram. The top and bottom of the gate run parallel to the x-axis while the sides of the gate follow the data and are slightly parabolic in nature. Bins, equally spaced slices of theta, are then applied to the data. When bins are prematurely cut off the statistics for that bin are not accurate. Examples of bins being prematurely cut off are, hardware thresholds such as the detector not physically covering that angle, user thresholds such as the joining of the scattering reactions making it impossible to resolve (d,d) data from (p,p) data, or situational thresholds such as the alpha contamination line running through into the (d,d) data. After the points that suffered from clipping where identified the bins within the usable angular range where divided in half. This doubled the points used in plotting the angular distribution and provided a more detailed plot. After excluding the invalid bins the angular range spanned by the data was 30.36°-43.31° in the center of mass frame, or 68.25°-74.75° in the lab frame.

Chapter 4

Results

4.1 Calibration Outcome

Previous energy calibration methods did a passable job of matching the front E detectors. Figure 4.1 shows an energy spectrum without any gains applied. Figure 4.2, in comparison is a sort of the same data with gains from the older method applied. It is clear that the peaks have shifted to a more acceptable energy. The peaks also became narrower and more sharply peaked. However, the older method still has not optimally gain matched that data as there is a small spread of channels amongst the peaks, i.e. an energy spread. The vast improvement of the newer method is clear when directly compared to the results of the older. Figure 4.3 depicts the newer method applied to the same two front E detectors as in figure 4.2. The peaks are clearly aligned at channel 1584, which in this plot corresponds to the 5.8 MeV alphas. The front E detectors had one dead strip on detector 2. Besides this strip all other strips were functional. When using the older method the gains for strip 2 on detector 2 were substantially bad. For this reason the results do not include strip two on detector two, even though the newer gain matching method produced gains that allowed the strip to be used. The two most important factors in judging the gains are centroid spread and energy resolution, or full width half maximum (FWHM). On average the older gains produced peaks with FWHM values of 46.05 channels. The older method also produced a centroid spread of 90.5 channels. In comparison the new method produced an average FWHM value of 25.17 and a centroid spread of 3.5 channels. The new method reduced the

average FWHM value by 20.89 channels or 76 KeV. Figures 4.4 and 4.5 show that similar improvements were seen with the PSD and the back angle detectors, respectively.

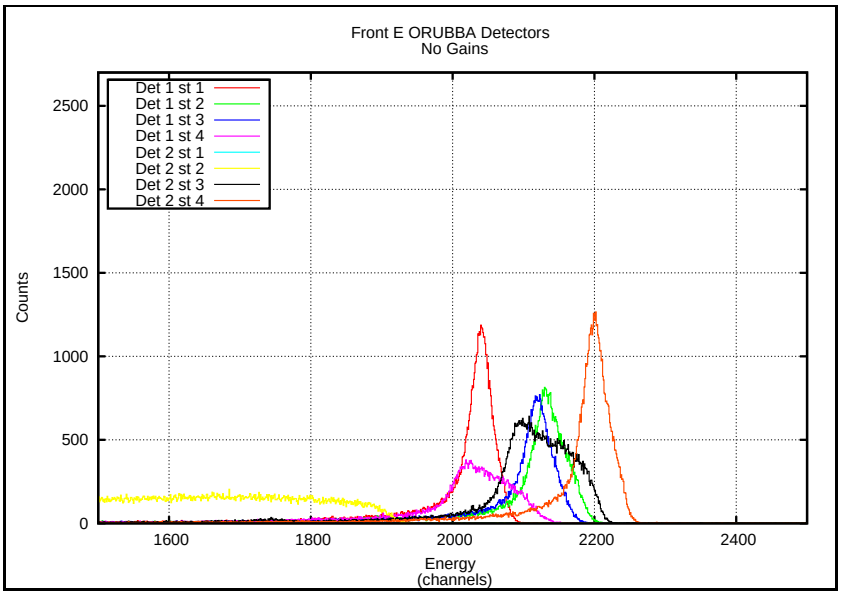

Figure 4.1: Energy Spectrum of the strips 1 through 4 for the first two forward angle detectors, with no gains applied.

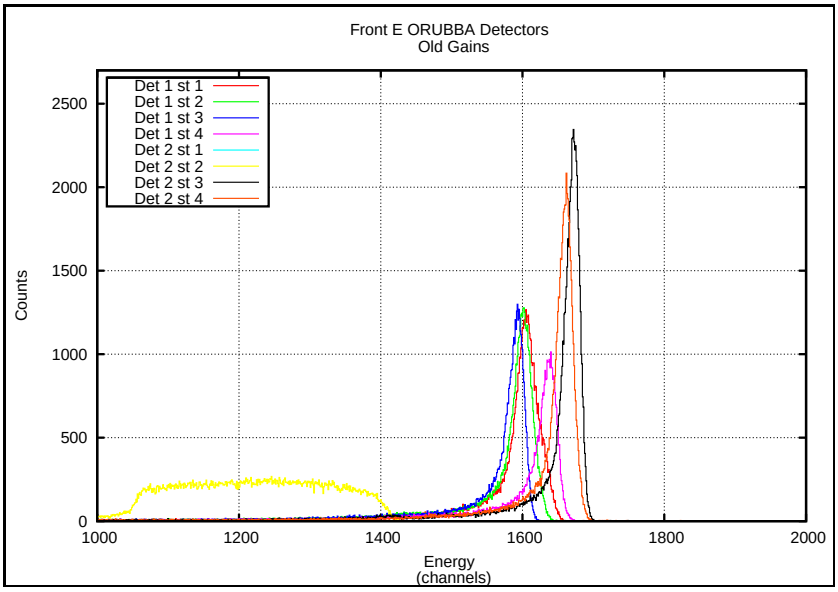

Figure 4.2: Energy Spectrum of the strips 1 through 4 for the first two forward angle detectors, using gains obtained through the older method.

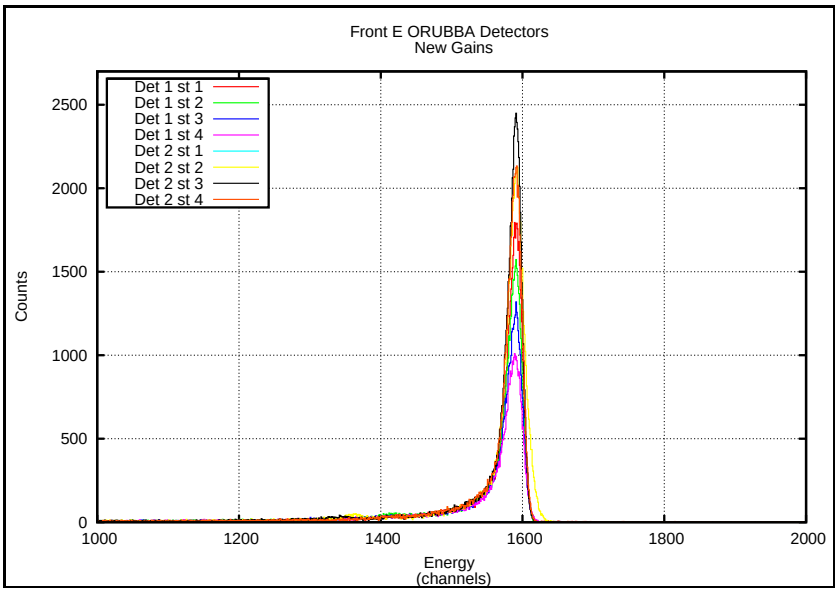

Figure 4.3: Energy Spectrum of the strips 1 through 4 for the first two forward angle detectors, using gains obtained through the new method.

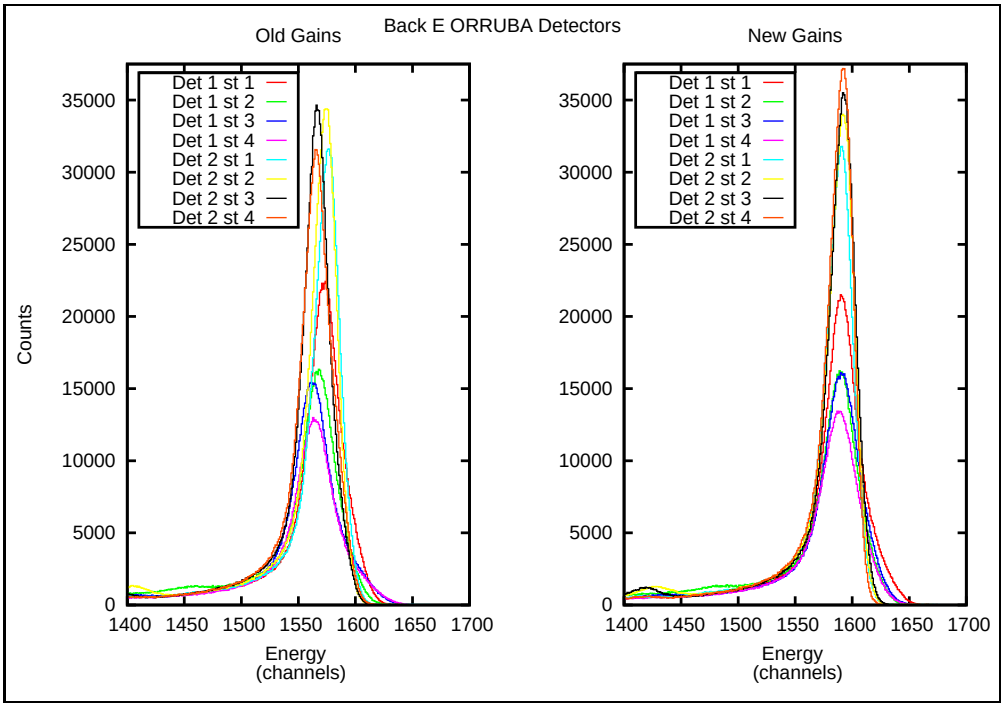

Figure 4.4: A comparison of the old gain methods results and new methods results using the Back E detectors.

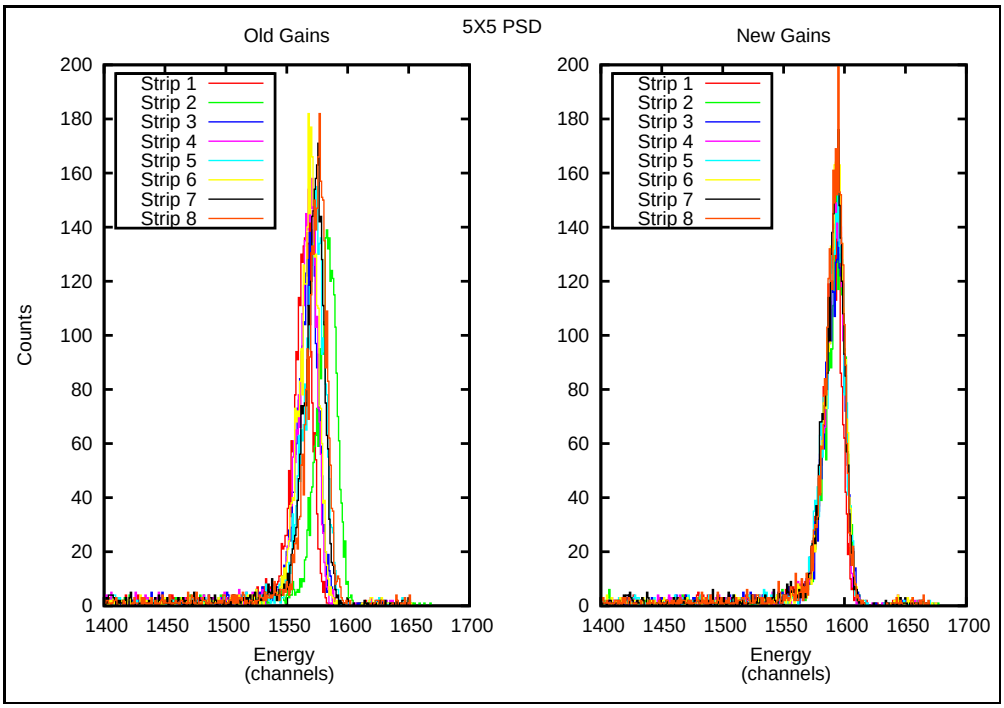

Figure 4.5: A comparison of the old gain method results and the new methods results using the 5x5 PSD. (8 out of 16 strips are shown)

4.2 Elastic Scattering

The first step in the analysis was to plot the pure Rutherford calculations against the angular distributions. Using the equation for Rutherford scattering theory, equation 2.1, calculations were made using the correct values for the (d,d) reaction. This pure Rutherford plot is shown against the angular distribution for the (d,d) reaction in figure 4.6. While it is clear that the pure Rutherford calculation provides a reasonable description of the angular distribution, it does not fit it perfectly. At the lower end of the angular distribution it is $\sim$8% below the data. This discrepancy arises because the potential is not simply a Coulomb potential. This was surprising as it was assumed that at these forward angles, in the center of mass frame, the scattering would be purely Rutherford in nature. Calculations performed by Filomena Nunes confirmed that about 5%, i.e. more than half of the 8% discrepancy, was due to nuclear effects. Since more then pure Rutherford effects were being seen in the scattering a different approach was required. As mentioned previously an

optical potential is better suited to model the elastic scattering. Two optical models were used and compared with the (d,d) angular distribution. When using optical models there are a number of parameters that are included in the absorption term; essentially anything that is not elastic scattering is included in $W(r)$. Optical models can be described as either local or global. The elastic scattering can be broken into two parts: the incoming part, describing the reactants, and the outgoing part, describing the products of the reaction. In the global optical model the incoming part took into account that the deuteron may actually break up on approach because it is so weakly bound [JS70]. The outgoing part uses the Chapel Hill optical model [Var87]. For shorthand purposes this optical model will be referred to as CH89+JS. The local optical model used was the Stroemich optical potential [S^{+}77] optimized for ^{124}Sn scattering. This potential was developed and used to model elastic scattering data from eight nuclei; ^{124}Sn, ^{130}Te, ^{138}Ba, ^{140}Ce, ^{142}Nd, and ^{208}Pb. Filomena Nunes used these two optical potentials to calculate the elastic scattering to be compared with the measured elastic scattering. Figures 4.7 and figure 4.8 depict the data compared to the CH89+JS and Stroemich models respectively. Figure 4.9 compared the pure Rutherford, the CH89+JS, and the Stroemich calculations to the data. The angular range 33° to 40° was selected as the optimal range to fit out data to the calulations and to develop a scaling factor. At angles larger than 40° the optical models quickly diverge from each other and pure Rutherford. At angles smaller then 33° the deuteron and the proton scattering reactions begin to converge. There was not sufficient resolution to determine when protons began "leaking" into the deuteron angular bins. Within this angular range there was an average difference of 4.8% between the pure Rutherford calculation and the data. When compared to the CH89+JS and Stroemich potential based optical model calculations the average difference was reduced to 2.3% and 2.2%, respectively. Within the angular range a max difference of 10.3% between Rutherford and the data was at the datum point for 33.4°. This was reduced to 7.3% for either the CH89+JS or Stroemich calculations. The normalization factor for each model agreed to within 2% of each other, meaning that the normalization factor is model independent. This provides confidence in using this value to continue with the (d,p) analysis and extraction of spectroscopic factors.

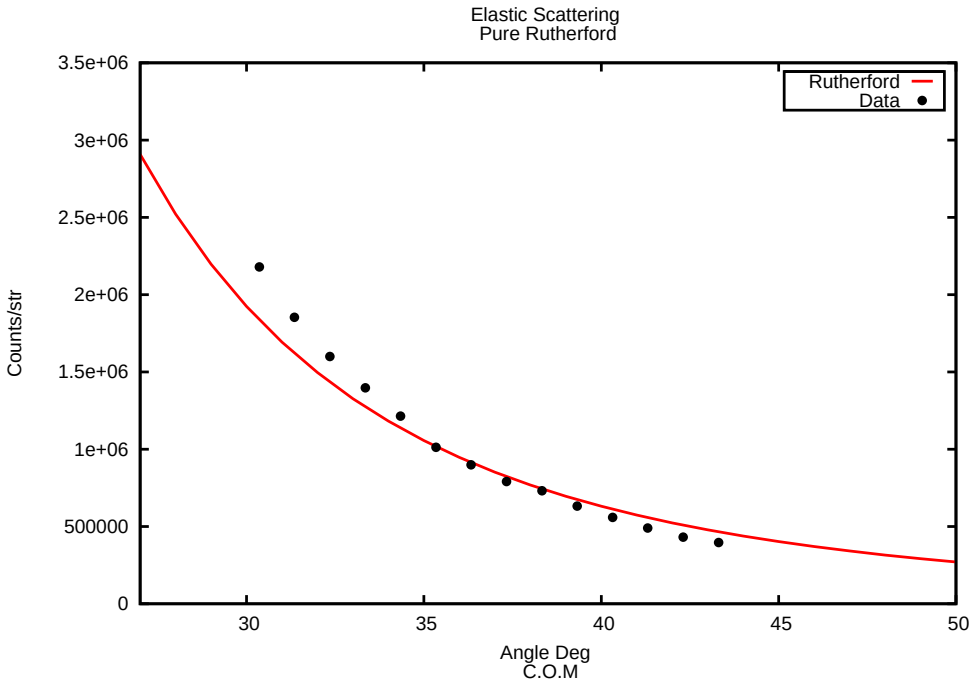

Figure 4.6: The data compared with the pure Rutherford calculation.

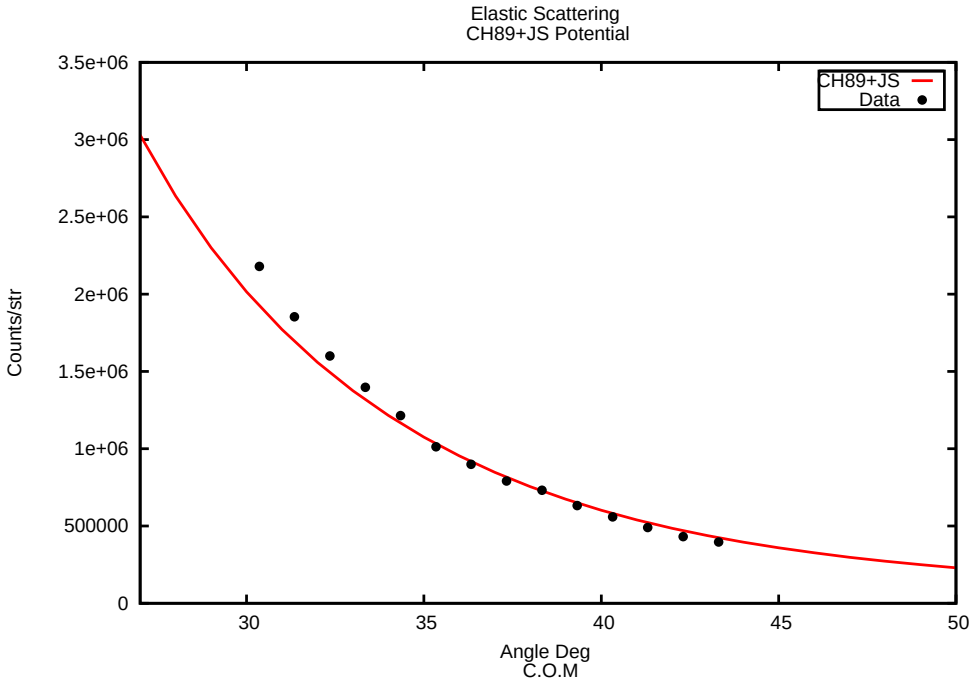

Figure 4.7: The data compared with the optical model based on the global CH89+JS optical potential.

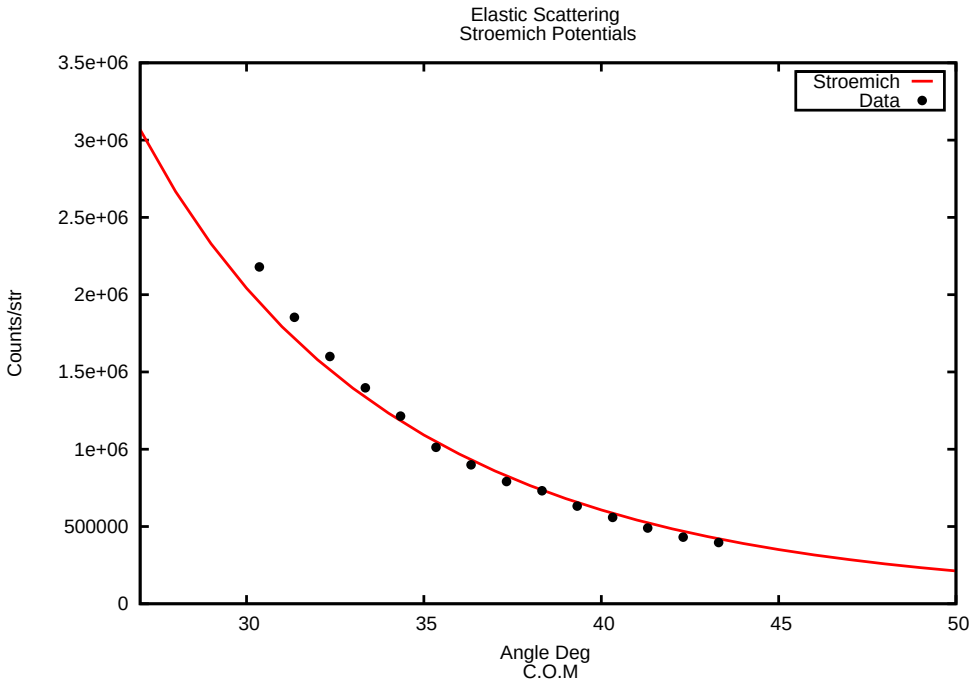

Figure 4.8: The data compared with the optical model based on the local Stroemich optical potential.

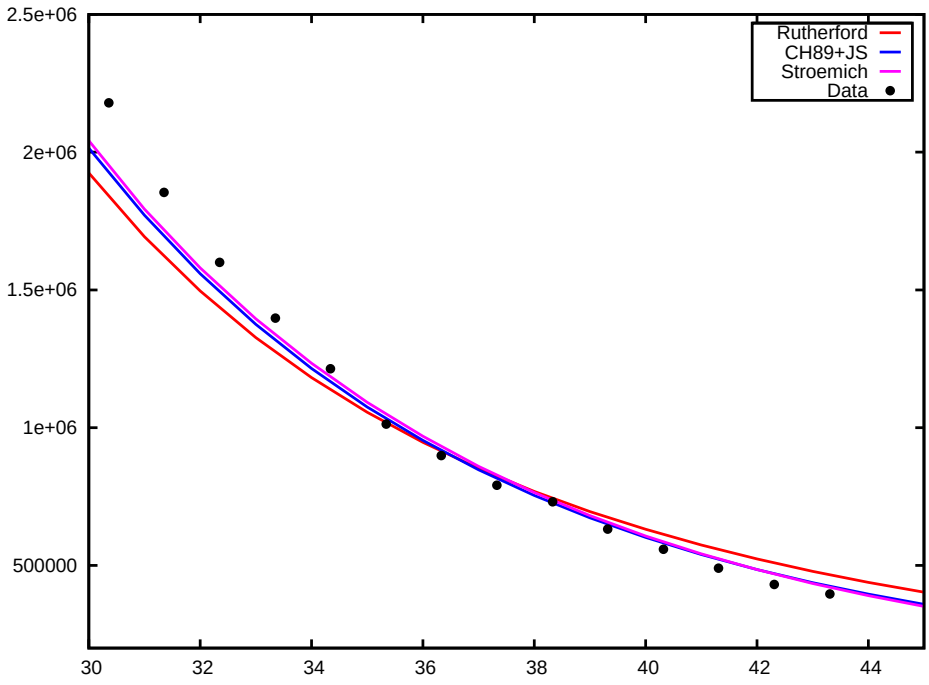

Figure 4.9: A close up comparison for the data with the Rutherford and the optical models.

Chapter 5

Conclusions

5.1 Gain Matching

A new gain-matching routine procedure was required for the newly implemented ORRUBA detector system. The old methods were not optimized for ORRUBA and suffered from user bias. RKUSF was written to replace the older methods and designed to work with ORRUBA detectors. Gain matching with RKUSF produced an improvement in FWHM from the old gains of 75 keV and reduced the centroid spread of the energy peaks form 90.5 channels to 3.5 channels. Currently RKUSF still requires relatively repetitive user inputs while running. Several methods have been considered for automating, the one most likely to be used is an evolution of RKUSF from a simply Fortran program to a Python program. Currently the gains are simply written to screen or a file depending on user preference. A universal output system was difficult because different scan codes can require the gains to be in different formats, also detector setup and identification can be unique for each experiment. Using a graphical user interface (GUI) written in Python the idea of implementing a soft template for writing out the gains is a very attractive idea for making RKUSF more adaptable for working with other experimental setups. RKUSF has been broken down into modules. Using a Fortran to Python interface generator, F2PY, these modules can be called the GUI which the user will be interacting with. However, this Python evolution is paused at the moment due to the developments in Python. The third generation of the Python language was recently released and is not 100 percent backwards

compatible with the widely used Python 2.x language. This could hamper some long-term usage of RKUSF; therefore until it is clear which direction the Python community is heading no decision on which generation of language to use will be made for RKUSF. Regardless of the future of RKUSF, the significant improvements that it provided in gain matching ORRUBA allowed for confident analysis of both the elastic scattering data and the (d,p) data.

5.2 Elastic Scattering

Elastic scattering of ^{132}Sn on deuterons was measured concurrently with a ^{132}Sn(d,p) measurement. The (d,d) data was initially compared to Rutherford Scattering and variances of up to 8% were found. Since it was surprising that the data differed from the calculation in the angular range it was decided the next step was to compare the data to a global optical model. The global optical potential compared much more favorably to the scattering data, however it still differed at the low end of the angular range. When a local potential by Stroemich et al was compared to the data, the fit was improved over the global model. Within the selected angular range mentioned in previous section there was an average difference of 4.8% between the pure Rutherford calculation and the data. When compared to the CH89+JS and Stroemich potential based optical model calculations the average difference was reduced to 2.4% and 2.2%, respectively. A max difference of 10.3% between Rutherford and the data was observed at the datum point for 33.4°. This was reduced to 7.3% when compared to the CH89+JS or Stroemich calculations. The normalization factor for each model agreed to within 2% of each other, showing that the normalization factor is model independent. The elastic scattering analysis has helped in the selection of the Stroemich potential based optical model for further (d,p) analysis and the normalization factor will be used to extract spectroscopic factors.

Bibliography

Bibliography

[B+00] D. W. Bardayan et al. "The astrophysically important 3^+ state in ^{18}Ne and the $^{17}f(p,\gamma)^{18}$Ne stellar rate". *Phys. Rev. C*, 62(5), Oct 2000.

[B+08] J. Beun et al. "Neutron capture on ^{130}Sn during r-process freeze-out". http://www.citebase.org/abstract?id=oai:arXiv.org:0806.3895, 2008.

[HRI] HRIBF. http://www.phy.ornl.gov/hribf/.

[J+08] K.L. Jones et al. "Studies of nuclei close to ^{132}Sn using single-neutron transfer reaction". submitted to Fusion 08, 2008.

[JS70] R. C. Johnson and P. J. R. Soper. "Contribution of Deuteron Breakup Channels to Deuteron Stripping and Elastic Scattering". *Phys. Rev. C*, 1(3), Mar 1970.

[Kra88a] K. Krane. *Inroductory Nuclear Physics*, chapter 5. "John Wiley and Sons", second edition, 1988.

[Kra88b] K. Krane. *Inroductory Nuclear Physics*, page 118. "John Wiley and Sons", second edition, 1988.

[Kra88c] K. Krane. *Inroductory Nuclear Physics*, chapter 19. "John Wiley and Sons", second edition, 1988.

[Kra88d] K. Krane. *Inroductory Nuclear Physics*, chapter 11. "John Wiley and Sons", second edition, 1988.

[P+07] S.D. Pain et al. "Development of a high solid-angle silicon detector array for measurement of transfer reactions in inverse kinematics". *Nuclear Instruments*

and Methods in Physics Research Section B: Beam Interactions with Materials and Atoms, 261(1-2):1122 – 1125, 2007.

[PTVF92] W.H. Press, S. A. Teukolsky, W. T. Vetterling, and B. P. Flannery. *NUMERICAL RECIPES in Fortran 77*. "Cambridge University Press", second edition, 1992.

[RR88] C. E. Rolfs and W. S. Rodney. *Cauldrons in the Cosmos*. "The University of Chicago Press", 1988.

[S+77] A. Strömich et al. "(d, p) reactions on ^{124}Sn, ^{130}Te, ^{138}Ba, ^{140}Ce, ^{142}Nd, and ^{208}Pb below and near the Coulomb barrier". *Phys. Rev. C*, 16(6), Dec 1977.

[S+08] R. Surman et al. "Neutron Capture Rates near A=130 which Effect a Global Change to the r-Process Abundance Distribution". http://www.citebase.org/abstract?id=oai:arXiv.org:0806.3753, 2008.

[Sat90] G. R. Satchler. *Introdution to Nuclear Reactions*. "Oxford University Press", second edition, 1990.

[Var] R. L. Varner. program spkhis. Unpublished.

[Var87] R.L. Varner. "Global parameterization of the nucleon-nucleus scattering potential". *Phys. Rev. B*, 185(1,2), Feb 1987.

Vita

Ryan Kapler was born on May 27, 1983 in Huntington, New York. In the fall of 2005 he enrolled at the University of North Carolina at Asheville, earning his Bachelor's of Science in Physics and a minor in Mathematics in the fall of 2005. His academic career continued as he was awarded a teaching assistantship and enrolled at the University of Tennessee the following fall. He graduated with a Master of Science degree in the field of Experimental Nuclear Physics in the spring semester of 2009.